High-pressure–high-temperature equation of state of KCl and KBr

A. Dewaele,[1] A. B. Belonoshko,[2] G. Garbarino,[3] F. Occelli,[1] P. Bouvier,[3,4] M. Hanfland,[3] and M. Mezouar[3]

[1]*CEA de Bruyères-le-Châtel, 91297 Arpajon Cedex, France*

[2]*Condensed Matter Theory, Department of Theoretical Physics, AlbaNova University Center, KTH Royal Institute of Technology, 106 91 Stockholm, Sweden*

[3]*European Synchrotron Radiation Facility, Boîte Postale 220, 38043 Grenoble Cedex, France*

[4]*Laboratoire des Matériaux et du Génie Physique, CNRS, Grenoble Institute of Technology, 3 parvis Louis Neel, 38016 Grenoble, France*

(Received 11 April 2012; published 6 June 2012)

The equation of state of KCl and KBr, compressed in a helium pressure medium in a diamond-anvil cell, has been measured by x-ray diffraction in the B1 and B2 phases up to 165 GPa at 298 K. The P-V-T of B2 KCl and B2 KBr has been calculated by *ab initio* molecular dynamics in a wide compression range and up to 7000 K. The thermal pressure exhibits a linear behavior with temperature and remains low under high compression. The experimental P-V points and the thermal pressure calculated by molecular dynamics have been used to set up a high-pressure–high-temperature equation of state of B2 KCl and B2 KBr. With these equations of state, B2 KCl and B2 KBr can be used as pressure markers in laser-heated diamond-anvil-cell experiments.

DOI: 10.1103/PhysRevB.85.214105 PACS number(s): 62.50.−p, 64.30.Jk, 71.15.Pd

I. INTRODUCTION

Alkali halides (NaCl, KCl, KBr, etc.) are used in high-pressure devices as pressure-transmitting media and pressure gauges.[1,2] Their advantages are softness, which reduces nonhydrostatic stress around the sample; chemical inertness, which prevents contamination of the sample during experiments; high compressibility, which increases their accuracy as x-ray pressure gauges; and simple crystal structure [B1 ($Fm3m$) phase at low pressure and B2 ($Pm3m$) phase at high pressure], which limits the number of parasitic x-ray diffraction peaks in a high-pressure experiment. If NaCl is the most popular of the alkali halides,[2] KCl and KBr appear now as interesting alternatives as they have a higher melting point, which makes them particularly useful as pressure-transmitting and thermal insulating media in laser-heated diamond-anvil-cell experiments.[3,4] It is thus necessary to establish a reference P-V-T equation of state (EOS) for KCl and KBr up to megabars and several thousand degrees Kelvin.

The phase stability and EOS data published for KCl and KBr are limited to typically 50 GPa and several hundred degrees Kelvin. KCl and KBr both undergo a B1 to B2 phase transformation around 2 GPa.[5] In fact, the B2 phase is favored for high r_C/r_A ratios (r_C and r_A are the radii of cations and anions), which increases with pressure because the compressibility of anions is larger than the compressibility of cations. Further transformation to a lower symmetry structure has been reported for Cs halides at a compression of $V/V_0 \simeq 0.5$;[6] however, no phase transformation is expected for alkali halides with a lighter cation such as KCl and KBr in the same compression range.[7] B2 KCl and B2 KBr EOS have been measured up to 56 GPa (Ref. 8) and 40 GPa,[9] respectively, in a diamond-anvil cell, but without any pressure-transmitting medium. Subsequent nonhydrostatic stress and pressure gradients have caused a large scatter and possibly a systematic bias in the P-V data. In the only high-temperature EOS study we are aware of, B2 KCl has been heated to 873 K and compressed up to 8 GPa.[10]

In this article, we report high-precision measurements of the ambient temperature EOS of KCl and KBr up to 165 GPa. In addition, the high-pressure–high-temperature EOS of these alkali halides has been calculated using *ab initio* molecular dynamics. The interests of combining first-principles and experimental approaches to obtain a more reliable description of the behavior of materials under high pressure and high temperature have been reviewed recently.[11] Using this synergy, the two methods are combined to obtain a P-V-T EOS suitable for pressure calibration purposes in laser-heated diamond-anvil-cell experiments.

II. AMBIENT T COMPRESSION CURVE

The diffraction experiments have all been performed with a similar sample geometry. KCl and KBr single-crystal samples (Fluka and Aldrich products, 99.5%+ purity) with thickness smaller than the space between the two diamond anvils under pressure were loaded in diamond-anvil cells together with ruby, which was used as a pressure gauge. Due to the hygroscopy of these halides, the samples were heated at 550 K in a vacuum oven prior to loading. Three of the diamond-anvil cells were loaded in an inert atmosphere using an argon glove box with partial content of oxygen and water below 0.1 ppm. The two remaining cells were loaded in air. No effect of the loading conditions was observed in the EOS measurements. Helium was used as pressure-transmitting medium. The ruby gauge calibration has been taken from Ref. 12. The monochromatic x-ray signal diffracted by the samples has been collected on a MAR555 imaging plate or a MAR CCD, located at a distance of ≃400 mm from the sample, on the ID09a or ID27 beam lines of the European Synchrotron Radiation Facility. The diffraction geometry was determined using a silicon or a LaB_6 reference sample. At each pressure step, the x-ray diffraction signal from the KCl and the KBr samples was recorded separately by small translations of the diamond-anvil cell; the pressure was measured before and after x-ray exposure. For each compound, two to five x-ray diffraction peaks were used to obtain the lattice parameter and volume per formula unit ($V_{B1} = a_{B1}^3/4$; $V_{B2} = a_{B2}^3$). The X-ray diffraction peaks corresponding to the (100), (200), and (210) reflections have not been taken into account in this calculation

TABLE I. Measured P-V points for B2 KCl and B2 KBr at 298 K. For each compound, five experimental runs have been performed; the data corresponding to each run are separated by an empty line. The uncertainty on pressure, measured with the ruby luminescence gauge,[12] is smaller than 2% up to 162 GPa;[13] the relative uncertainty on volume is smaller than 10^{-3} below 50 GPa and 5×10^{-3} above 50 GPa.

B2 KCl						B2 KBr					
P (GPa)	V(Å^3)	P (GPa)	V(Å^3)	P (GPa)	V(Å^3)	P (GPa)	V(Å^3)	P (GPa)	V(Å^3)	P (GPa)	V(Å^3)
3.14	48.145			2.56	48.991	3.14	55.131	2.55	56.443	2.2	56.978
3.81	47.36	3.14	48.06	3.39	47.81	3.81	54.214	3.36	55.106	2.51	56.325
4.75	46.267	3.45	7.783	5.66	45.235	4.75	52.796	3.59	54.599	3.33	54.865
5.54	45.423	3.82	47.33	5.66	45.247	5.54	51.743	3.92	54.143	5.63	51.587
7.03	44.093	5.72	45.208	6.45	44.501	7.03	50.089	6.22	51.034	6.34	50.762
8.85	42.726	5.72	45.208	7.86	43.316	8.85	48.403	6.52	50.662	7.74	49.296
10.1	41.832	6.13	44.806	9.17	42.344	10.1	47.384	8.62	48.616	9.04	48.113
11.9	40.79	6.13	44.799	10.8	41.287	11.9	46.136	9.46	47.901	10.6	46.914
13.5	39.906	6.44	44.505	12.3	40.42	13.5	45.046	10.1	47.433	12.2	45.797
15.9	38.749	8.47	42.956	14.2	39.416	15.9	43.742	11.6	46.376	14.1	44.599
18.4	37.774	9.39	42.279	15.6	38.765	18.4	42.446	14.3	44.632	15.4	43.808
20.7	36.866	10.0	41.801	17.5	37.788	20.7	41.495	15.0	44.201	17.4	42.786
22.9	36.083	11.4	41.016	19.8	37.016	22.9	40.512	16.9	43.252	19.6	41.774
25.9	35.214	13.9	39.566	22.4	36.241	25.9	39.444	24.1	40.094	22.3	40.677
28.4	34.555	14.9	39.178	26.1	34.916	28.4	38.76	27.7	38.921	26	39.376
31.2	33.875	23.9	35.813	28.5	34.314	31.2	37.93	33.3	37.306	28.4	38.615
34.3	33.134	27.5	34.721	31.5	33.63	34.3	37.105	37.4	36.264	31.4	37.742
37.0	32.605	32.9	33.333	34	33.09	37	36.459	41.9	35.252	33.8	37.096
		37.2	32.425	37.1	32.37			47.2	34.423	36.9	36.334
22.7	36.216	41.7	31.539	41.1	31.639	22.7	40.614	52.2	33.542	40.9	35.44
28.5	34.702	47.0	30.701	45.1	31.001	28.5	38.873	56.9	32.737	45	34.622
36.2	32.849	51.8	29.994	45.4	30.98	36.2	36.685	62.7	31.909	45.3	34.578
41.6	31.758	56.7	29.339	49.4	30.246	41.6	35.533	67.4	31.31	49.3	33.816
48	30.643	62.5	28.619	53.4	29.666	48.0	34.32	71.4	30.822	53.3	33.156
53.8	29.827	67.2	28.076			54	33.391	75.3	30.304		
58.6	29.236	71.2	27.663			58.8	32.658	75.6	30.279	2.68	56.046
65.1	28.435	75.3	27.213	2.78	48.656	65.1	31.763	79.4	29.999	3.27	54.985
70.3	27.861	75.6	27.186	3.31	47.964	70.3	31.049	83.2	29.594	3.85	53.976
74.5	27.433	78.9	26.911	3.9	47.159	74.5	30.598	88.2	29.183	4.53	52.998
79.6	27.027	82.9	26.565	4.59	46.353	79.6	30.107	92.2	28.801	5.43	51.775
86.7	26.409	87.8	26.187	5.53	45.369	86.7	29.318	96.7	28.428	7.46	49.554
92.2	25.998	92.1	25.866	7.57	43.554	92.2	28.799	100	28.149	7.9	49.108
97.8	25.719	96.6	25.538	7.93	43.214	97.8	28.342	105	27.766	8.24	48.814
103	25.20	99.9	25.293	8.3	42.968	103	27.962	105	27.763	9.58	47.665
111	24.737	105	24.963	9.66	42.019	111	27.397	107	27.601	11.2	46.481
118	24.361	105	24.959	11.2	41.018	118	26.961	109	27.464	12.3	45.804
125	23.881	106	24.834	12.1	40.48	125	26.52	110	27.436	12.2	45.771
132	23.553	109	24.69	12.3	40.421	132	26.109			13.8	44.822
138	23.251	110	24.664	13.9	39.583	138	25.725			14	44.618
144	23.003			14.1	39.472	144	25.374			15.7	43.671
152	22.717			15.9	38.661	152	24.961			17.7	42.719
157	22.452			17.8	37.855	157	24.78			19.5	41.901
161	22.252			19.5	37.161	162	24.547			20.4	41.515
165	22.065			20.5	36.844	165	24.414				

because we noticed that they yield systematically higher lattice parameters than other lines above $\simeq$50 GPa. It is known that these peaks are the most affected by nonhydrostatic stress in diamond-anvil-cell EOS measurements.[14] Nonhydrostatic stress was thus measurable in the helium pressure medium above $\simeq$50 GPa in these experiments, confirming earlier findings;[14] their effect was diminished by the selection of the diffraction lines used to calculate the sample volume. A total of 170 data points have been recorded for each alkali halide.

KCl and KBr undergo the B1 to B2 phase transformation at 2.6 and 2.3 GPa, respectively, with an 11.5% volume discontinuity, and remain in this phase up to the maximum pressure reached (165 GPa). No pressure domain in which the B1 and B2 phases coexist was observed.

The measured P-V points are listed in Tables I and II and are plotted in Figs. 1 and 2. They have been fitted with a Rydberg-Vinet[15] EOS in the B1 and B2 phases, leading to the parameters V_0, K_0, and K_0' (volume, bulk modulus, and

TABLE II. Measured P-V points for B1 KCl and B1 KBr at 298 K.

B1 KCl		B1 KBr	
P (GPa)	V(Å^3)	P (GPa)	V(Å^3)
0.72	60.263	0.7	69.031
1.32	58.57	1.3	66.804
2.0	57.001	1.9	64.771
2.5	55.856	2.5	63.409
0.20	61.698	0.2	71.013
0.29	61.412	0.27	70.653
0.44	60.857	0.43	69.949
0.57	60.513	0.54	69.481
0.85	59.785	0.79	68.568
1.2	58.991	1.07	67.529
1.4	58.38	1.4	66.635
1.5	58.127	1.46	66.292
1.7	57.742	1.64	65.817
1.8	57.337	1.8	65.28
2.1	56.742	2.1	64.536
2.4	56.271	2.3	63.933
0.16	61.704	0.16	71.043
0.27	61.322	0.26	70.517
0.37	61.038	0.36	70.145
0.64	60.193	0.64	69.005
0.9	59.513	0.86	68.186
1.34	58.428	1.3	66.753
1.64	57.762	1.6	65.914
2.24	56.489	2.2	64.296
2.56	56.075		
		1.0	67.248
1.0	58.889	1.1	67.276
1.08	58.861	1.8	65.002
2.12	56.585	2.2	64.29
2.3	56.293	2.3	63.933
2.40	56.063	2.4	63.683

its pressure derivative under ambient conditions, respectively) summarized in Table III. For the B2 phase, V_0, K_0, and K_0' are fictive parameters the phase would have at ambient pressure if stable in the same form. The current EOS parameters are very close to the ultrasonic ones for the B1 phase. In our study, the bulk modulus is 17.1 and 14.2 GPa for B1 KCl and B1 KBr, respectively; ultrasonic bulk moduli are 17.35 and 14.64 GPa.[9] For B2 KBr, the agreement with Ref. 9 diamond-anvil-cell measurements is good when a trade-off between K_0 and K_0' is corrected. The discrepancy with Refs. 8 and 10 for B2 KCl bulk modulus is more obvious ($\simeq$30% difference in K_0). However, the P-V points reported in Refs. 8 and 10 are in correct agreement with ours (see Fig. 1); we thus believe that the differences in EOS parameters may be attributed to the different scanned pressure ranges and different functional forms used, which led to different elastic parameters when extrapolated to ambient pressure, out of the stability range of the B2 phase.

The residuals $\Delta V = V_{\rm exp} - V_{\rm RV\ fit}$ plotted in Figs. 1 and 2 for B2 KCl and B2 KBr exhibit a clear nonmonotonic trend; ΔV first increases up to $\simeq$15 GPa and progressively decreases above that pressure. This is an indication that the B1-B2 phase transformation affects the bulk modulus of the B2 phase; it is higher just above the phase transformation, as

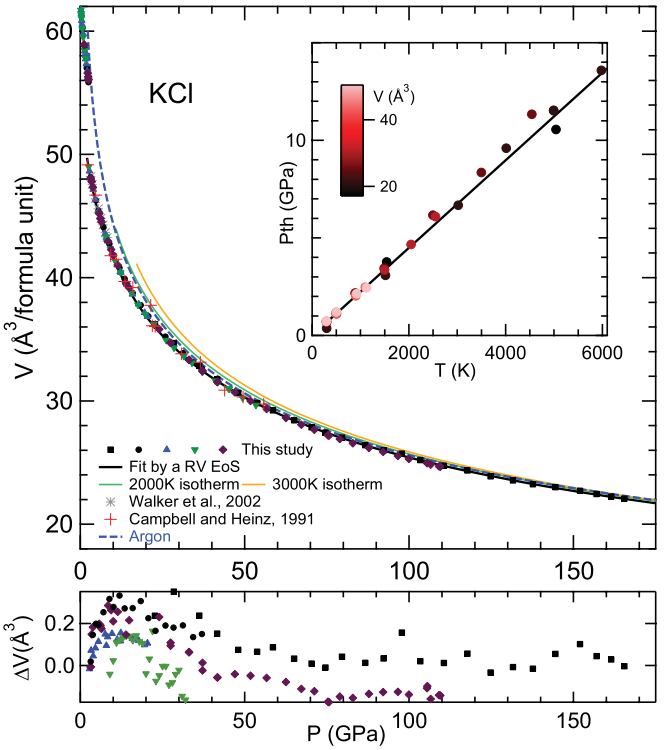

FIG. 1. (Color online) (top) Experimental P-V points measured for KCl at 298 K, with a Rydberg-Vinet (RV)[15] fit. Two high-temperature isotherms, calculated using Eq. (2) with Table V parameters, are also represented. The 298 K equation of state of argon[18,19] is plotted for comparison. The inset shows the thermal pressure calculated in the B2 phase by molecular dynamics; it can be fitted by $P_{\rm th} = \overline{\alpha K_T} T$. (bottom) Residuals $\Delta V = V_{\rm exp} - V_{\rm RV\ fit}$ for the B2 phase.

expected for pressure-induced phase transitions. The scatter of ΔV gives an indication of the accuracy of the volume measurements (typically 10^{-3}), and the difference between different experimental runs is due to different calibrations of wavelength between different experimental runs.

It has been noted in previous studies that the EOS of some ionic crystals is very close to the EOS of isoelectronic rare-gas solids: CsI and Xe (Ref. 16) and LiH and He.[17] We make a similar observation here: the EOS of KCl progressively converges with the EOS of isoelectronic argon when the pressure is much higher from the B1 to B2 phase transformation pressure, which significantly affects the bulk modulus. The EOS of argon plotted in Fig. 1 has been obtained using the published P-V data,[18,19] corrected according to a more recent ruby pressure calibration.[12,20] The corrected P-V points can be fitted by the sum of a Rydberg-Vinet[15] EOS at 0 K ($V_0 = 37.862$ Å^3, $K_0 = 2.65$ GPa, $K_0' = 7.57$) and a thermal pressure term taken from Ref. 19. The convergence of the EOS of KCl and argon is somewhat surprising, as the packing in argon, a face-centered-cubic crystal, is different from the packing in KCl. On the other hand, this may suggest that the repulsive interactions are similar in these two solids.

The calculations of the total energies were done by the projector augmented-wave (PAW) method[21] (as implemented in VASP[22]) based on the density functional theory (DFT). Exchange and correlation potentials were treated within the Wang

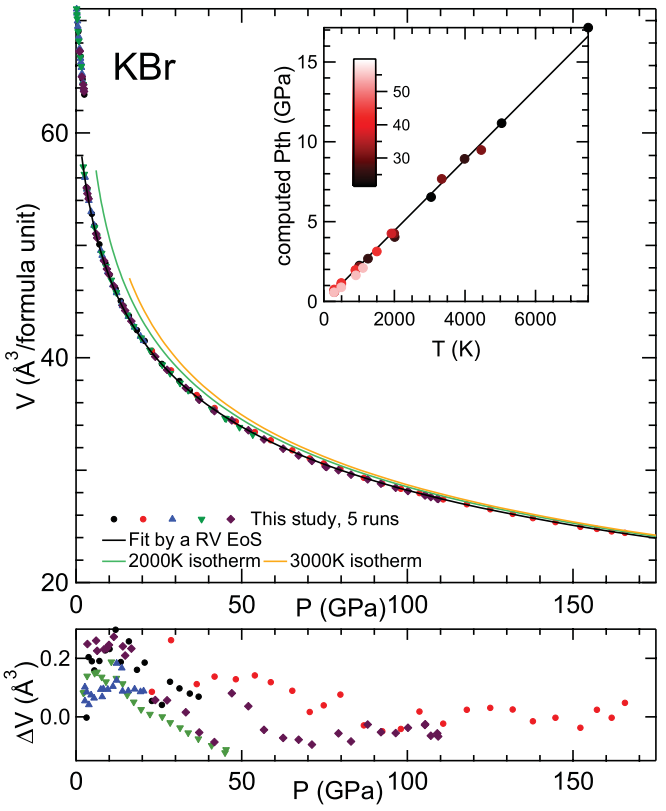

FIG. 2. (Color online) (top) Experimental P-V points measured for KBr at 298 K, with a Rydberg-Vinet (RV)[15] fit. Two high-temperature isotherms, calculated using Eq. (2) with Table V parameters, are also represented. The inset shows the thermal pressure calculated in the B2 phase by molecular dynamics; it can be fitted by $P_{\text{th}} = \overline{\alpha K_T} T$. (bottom) Residuals $\Delta V = V_{\text{exp}} - V_{\text{RV fit}}$ for the B2 phase.

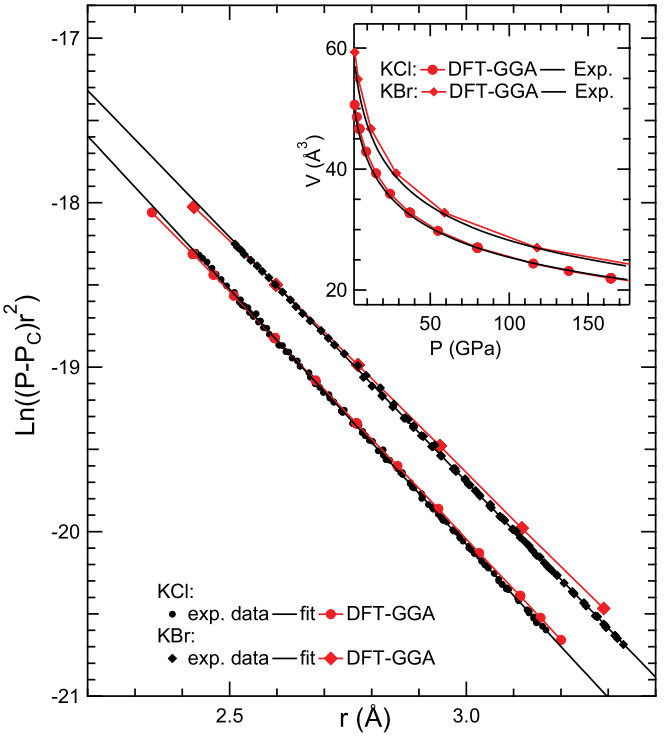

FIG. 3. (Color online) Plot of $\ln[(P - P_C)r^2]$ (P_C is the Coulombic interaction pressure) vs the cation-anion distance r for B2 KCl and B2 KBr. Experimental data (black points) and DFT-GGA (red points) P-V points have been used. The inset shows a comparison between 0 K P-V points from the DFT-GGA calculations (see Table IV) and the 298 K experimental compression curve.

and Perdew generalized gradient approximation (GGA).[23] The calculations were performed considering nine valence electrons for K and seven valence electrons for Br and Cl. Core radii were 2.3 Å. The finite temperatures for the electronic structure and force calculations were implemented within the Fermi-Dirac smearing approach.[24] The cutoff energies were set to 20.58 and 19.05 Ry for KCl and KBr, respectively. The Γ point was used in all calculations. It was sufficient due to the large supercell we used. The structure of KCl and KBr in all our calculations was B2.

P-V points at 0 K obtained for KCl and KBr are listed in Table IV. They could be fitted with a Rydberg-Vinet[15] EOS, with the following V_0, K_0, and K_0' parameters: 55.605 Å^3/f.u., 17.4 GPa, and 5.63, respectively, for KCl and 66.17 Å^3/f.u., 13.8 GPa, and 5.65, respectively, for KBr (Table III). They compare reasonably well with the experimental EOS parameters, and the P-V plots are almost indistinguishable (see Fig. 3).

TABLE III. The 298 K EOS parameters for both phases of KCl and KBr compared with the literature data. The experimental results from the current study are in bold. For the B1 phase, K_0' has been fixed to the value obtained by ultrasonic measurements. For the B2 phase, V_0 has been fixed to a value which is in agreement with the lowest pressure (2–6 GPa) measurements. RV: Rydberg-Vinet[15] [see Eq. (2)].

Phase	P range (GPa)	V_0 (Å^3/f.u.)	K_0 (GPa)	K_0'	Reference
KCl B1	0–2.6	**62.36**	**17.1**	**5.5** (fixed)	This work, RV EOS
KCl B1			17.35	5.46	Ref. 9, ultrasonic measurement
KCl B2	2.6–165	**54.5** (fixed)	**17.2**	**5.89**	This work, experiments, RV EOS
KCl B2	0–233	55.605	17.4	5.63	This work, DFT-GGA, RV EOS
KCl B2	4–8	53.53	23.7	4.4	Ref. 10, Birch-Murnaghan EOS
KCl B2	2.2–56	53.8	24.6	5.2	Ref. 8, RV EOS
KBr B1	0–2.3	**71.89**	**14.2**	**5.5** (fixed)	This work, RV EOS
KBr B1			14.64	5.47	Ref. 9, ultrasonic measurements
KBr B2	2.3–165	**63.4** (fixed)	**14.9**	**5.81**	This work, experiments, RV EOS
KBr B2	0–227	66.17	13.8	5.65	This work, DFT-GGA, RV EOS
KBr B2	3–43	62.93	17	5.38	Ref. 9, H11-EOS

TABLE IV. Lattice parameter a of B2 KCl and B2 KBr calculated by molecular dynamics as a function of temperature T and pressure P, using DFT-GGA. The error bars are 13% on P.

B2 KCl			B2 KBr		
a (Å)	T (K)	P (GPa)	a (Å)	T (K)	P (GPa)
2.7	0	233	2.8	0	227
2.8	0	164	2.8	1009	229
2.8	300	165	2.8	3039	233
2.8	1516	168	2.8	5037	238
2.8	3020	171	2.8	7493	244
2.8	4012	174	3.0	0	118
2.8	4991	176	3.0	297	118
2.8	4992	176	3.0	1248	120
2.8	5977	178	3.0	2005	122
2.85	0	138	3.0	3990	127
2.9	0	115	3.2	0	59
3.0	0	79.8	3.2	297	59
3.0	298	80.6	3.2	995	61.2
3.0	497	81.0	3.2	1994	63.3
3.0	890	82.0	3.2	3341	66.7
3.0	3496	88.2	3.2	4462	68.5
3.0	1488	83.3	3.2	5412	71.2
3.0	2495	86.0	3.2	5875	76.0
3.0	4540	91.2	3.4	0	28.3
3.1	0	54.9	3.4	293	28.9
3.2	0	37.0	3.4	495	29.4
3.2	502	38.1	3.4	897	30.3
3.2	296	37.7	3.4	1916	32.6
3.2	895	39.1	3.6	0	12.3
3.2	1499	40.3	3.6	293	13.1
3.2	2044	41.7	3.6	493	13.5
3.2	2551	43.1	3.6	896	14.3
3.3	0	24.5	3.6	1500	15.5
3.4	0	15.6	3.8	0	4.4
3.5	0	9.3	3.9	0	2.01
3.6	0	5.0	3.9	289	26.7
3.6	290	5.7	3.9	494	2.99
3.6	492	6.1	3.9	906	3.74
3.6	900	7.0	3.9	1109	4.20
3.6	1099	7.5			
3.65	0	3.4			

A more precise comparison between the experimental and the *ab initio* compression curves can be performed using the Born model for ionic solids. This model states that the interionic potential V can be split into two terms, a Coulombic term V_C and a repulsive term V_R,which are simple functions of the cation-anion distance r:

$$V(r) = V_C + V_R = M/r + Ae^{-Br}.$$

As a consequence, the pressure $P = -dU/dV$ is also the sum of a Coulombic term P_C and a repulsive term P_R: $P = P_R + P_C$. The repulsive pressure P_R should behave as $P_R \propto e^{-Br}/r^2$. We have thus calculated $\ln[(P - P_C)r^2]$ vs r for our experimental data and the GGA output. P_C was estimated using the Madelung constant for CsCl-type crystals (1.763). For the experimental data in B2 KCl and B2 KBr, the trend is a line, as expected with this form of the repulsive interaction. For the GGA points, the trend is slightly different, which suggests that the repulsive interaction is slightly underestimated by GGA under high compression and/or overestimated under low compression. Indeed, the values of K_0' listed in Table III show that the experimental cold compression curve becomes slightly stiffer than the GGA one at high compression. However, the difference between experimental and theoretical volumes at a given pressure remain smaller than 1.5% in the scanned pressure range; the Wang and Perdew GGA thus appears to be a good model of these ionic systems in this range.

III. THERMAL PRESSURE

A description of the molecular dynamics (MD) method can be found elsewhere.[25] Our MD simulations were performed in the microcanonical ensemble where N (number of atoms), V (volume), and E (energy) are conserved. Periodic boundary conditions have been applied. The time step for solving the differential equations of atomic motion was equal to 1 fs. This was checked by performing test calculations with the time step of 0.5 fs. The number of time steps in our MD simulations varied depending on temperature and was largest (8000 time steps) at high T; otherwise, 4000 time steps were used. This was found to be sufficient for obtaining good averages by calculating running averages. The number of atoms was 128. It is expected that this number gives reasonable results for the solid state not too close to melting. The MD run results are presented as long as the radial distribution function exhibits sharp peaks, so there is no evidence of melting. This suggests that the simulated states are below the melting curve; however, in some runs the solid might have been preserved metastably. The calculations have been performed at a number of volumes and temperatures, and the pressure P was calculated for each point. The pressures obtained at several lattice parameters and various temperatures are listed in Table IV.

Using this output, the thermal pressure,

$$\begin{aligned} P_{\rm th}(V,T) = {} & P(V,T) - P(V,T=0) \\ = {} & \int_0^T \left(\frac{\partial P}{\partial T}\right)_V dT = \int_0^T \alpha K_T dT, \end{aligned} \quad (1)$$

was calculated. In Eq. (1), α is the volumetric thermal expansion coefficient, and K_T is the isothermal bulk modulus, which both vary with V and T. We have estimated that the relative errors bars on $P_{\rm th}$ are lower than 13%.

In order to test the effect of the approximations in DFT on the thermal pressure, we have also performed a few MD runs using a different approximation of the exchange correlation for B2 KCl: the local-density approximation (LDA).[27] We obtained that $P_{\rm th}(V,T)$ calculated with LDA is within 10% (less than the error bars) of $P_{\rm th}(V,T)$ calculated within GGA. GGA and LDA constitute extreme models of the exchange-correlation interactions; all modern available functionals yield compression curves which are located between LDA and GGA, as noted for metals[13] and NaCl.[11] This result thus proves that the thermal pressure calculated by MD is insensitive to the choice of the exchange-correlation approximation and potential.

Thermal pressures are represented in the insets of Figs. 1 and 2, which show that the thermal pressure calculated in

TABLE V. Parameters of the P-V-T EOS [Eq. (2)] for B2 KCl and B2 KBr.

Compound	B2 KCl	B2 KBr
V_0 (Å^3/f.u.)	54.5	63.4
K_0 (GPa)	17.2	14.9
K_0'	5.89	5.81
$\overline{\alpha K_T}$ (GPa/K)	0.00224	0.00222

solid B2 KCl and B2 KBr is proportional to the temperature, within the error bars, in a compression range V/V_0 of 0.4 to 1 and between 300 and 7500 K. This suggests that Eq. (1) can be approximated by $P_{\text{th}}(V,T) \simeq \overline{\alpha K_T} T$, where $\overline{\alpha K_T}$ is a constant. In other words, no significant second-order derivative $(\partial^2 P/\partial T^2)_V$ or $(\partial^2 P/\partial T \partial V)$ could be extracted from $P_{\text{th}}(V,T)$. With the Debye temperatures of KCl and KBr being, respectively, 235 and 174 K under ambient conditions,[26] the scanned temperature range corresponds to the high-temperature limit for the Debye model. In this regime, it is expected that $(\partial^2 P/\partial T^2)_V = 0$ in the quasiharmonic approximation and that $(\partial^2 P/\partial T \partial V) = 0$ if, in addition, the Grüneisen parameter γ behaves as $d(\gamma/V)/dV = 0$. Such a simple behavior has been reported, on the basis of measurements, for several oxides[28] and for B1 NaCl (Ref. 29) above the Debye temperature. Recent MD simulations have also predicted an almost-constant value of αK_T for B2 NaCl.[30] A fit of P_{th} plotted in the insets of Figs. 1 and 2 yields $\overline{\alpha K_T} = 0.00224$ GPa/K for KCl and 0.00222 GPa/K for KBr. It should be noted that $\overline{\alpha K_T}$ of KCl and KBr is very low compared to its value in other solids used for pressure calibration purposes in a high-pressure–high-temperature apparatus: 0.0060 GPa/K for MgO,[28] 0.0067 GPa/K for gold at ambient volume,[31] 0.0065 GPa/K for platinum,[12] 0.0027 GPa/K for B1 NaCl,[29] and 0.0033 GPa/K for B2 NaCl.[30]

We have built a P-V-T EOS for B2 KCl and B2 KBr using our experimental ambient-temperature compression curves and the thermal pressure estimated using our MD runs. In this way, the usual bias of the density functional theory in the $P(V,T=0)$ curve estimation, related to the approximate calculation of the exchange-correlation term, is avoided. Indeed, the choice of this approximation leads to variations of 8% and 30%, respectively, on the equilibrium volume and bulk modulus.[11,13] On the experimental side, volumes are measured with an accuracy of a fraction of a percent, and the pressure measurement at ambient temperature with a ruby gauge is accurate within 2% up to 200 GPa.[13] The cold-compression curve is thus better constrained by experimental data. On the other hand, the thermal part of the equation of state depends less dramatically on the exchange-correlation approximation, as proven in this study. The precise experimental measurement of thermal pressure under high compression is difficult mainly because of the lack of an established pressure metrology under high temperature and the inhomogeneities of pressure and temperature in laser-heated diamond-anvil cells. The difficulties of pressure metrology under high temperature are illustrated by the differences between published calibrations of the MgO x-ray pressure gauge reviewed in Ref. 32. The approach of using a combination of experimental and computational outputs to build a high-pressure–high-temperature EOS has been successfully used in previous works.[33,34] We express here the total pressure as a sum of a Rydberg-Vinet[15] isothermal term obtained using 300 K measurements and a thermal pressure term under its simplest form:

$$P(V,T) = 3K_0\eta^{-2/3}(1-\eta^{1/3})\exp\left[\frac{3}{2}(K_0'-1)(1-\eta^{1/3})\right] + \overline{\alpha K_T} \times (T-300), \quad (2)$$

where $\eta = V/V_0$. The parameters listed in Table V have been used to calculate the isotherms plotted in Figs. 1 and 2. When compression increases, different isotherms become very close to each other; this trend can be observed in all solids, but it is particularly pronounced for KCl and KBr, which have a constant and particularly low $\overline{\alpha K_T}$ parameter. This lack of sensitivity of volume to temperature is a positive point for the use of KCl or KBr as x-ray pressure calibrants: at 100 GPa, an overestimation of the KCl temperature by 1000 K, which can happen in the pressure-transmitting medium in laser-heating experiments because of the large temperature gradients in this medium, would lead to an overestimation of pressure of only 1.5 GPa.

IV. CONCLUSION

In this work, a reference P-V-T equation of state has been established for B2 KCl and B2 KBr that is suitable for pressure calibration purposes in laser-heated diamond-anvil cells in the 0–200 GPa and 300–7000 K pressure-temperature range. The measurement of these pressure media specific volumes by x-ray diffraction allows pressure measurements with an accuracy of a few gigapascals under ultrahigh pressure, even in the presence of large temperature uncertainties due to the large temperature gradients often observed in this setup. This is due to their low thermal expansivity under pressure.

ACKNOWLEDGMENTS

Part of this work was performed at the European Synchrotron Radiation Facility (ESRF), Grenoble, France, under proposal HS-4328. J. Jacobs and H. Muller are acknowledged for the preparation of pressure cells and for the use of the glove box. S. Anzellini is acknowledged for experimental help. We thank P. Loubeyre for his interest in this project. Computations were performed using the facilities of the National Supercomputer Center in Linköping. A.B. thanks the Swedish Research Council (VR).

[1] D. L. Decker, J. Phys. Chem. Ref. Data **1**, 773 (1972).
[2] K. Syassen and W. B. Holzapfel, J. Appl. Phys. **49**, 4427 (1978).
[3] A. Dewaele, M. Mezouar, N. Guignot, and P. Loubeyre, Phys. Rev. Lett. **104**, 255701 (2010).
[4] G. Morard, D. Andrault, N. Guignot, J. Siebert, G. Garbarino, and D. Antonangeli, Phys. Chem. Miner. **38**, 767 (2011).
[5] M. Flórez, J. M. Recio, E. Francisco, M. A. Blanco, and A. M. Pendás, Phys. Rev. B **66**, 144112 (2002).

[6]Y. K. Vohra, S. J. Duclos, and A. L. Ruoff, Phys. Rev. Lett. **54**, 570 (1985).
[7]M. Buongiorno Nardelli, S. Baroni, and P. Gianozzi, Phys. Rev. B **51**, 8060 (1995).
[8]A. J. Campbell and D. L. Heinz, J. Phys. Chem. Solids **52**, 495 (1991).
[9]U. Kohler, P. G. Johannsen, and W. B. Holzapfel, J. Phys. Condens. Matter **9**, 5581 (1997).
[10]D. Walker, L. M. D. Cranswick, P. K. Verma, S. M. Clark, and B. Buhre, Am. Mineral. **87**, 805 (2002).
[11]S. Ono, in *Some Applications of Quantum Mechanics* (Intech, Vienna, 2012), pp. 91–108.
[12]P. I. Dorogokupets and A. R. Oganov, Phys. Rev. B **75**, 024115 (2007).
[13]A. Dewaele, M. Torrent, P. Loubeyre, and M. Mezouar, Phys. Rev. B **78**, 104102 (2008).
[14]K. Takemura and A. Dewaele, Phys. Rev. B **78**, 104119 (2008).
[15]P. Vinet, J. Ferrante, J. H. Rose, and J. R. Smith, J. Geophys. Res. **92**, 9319 (1987).
[16]A. N. Zisman, I. V. Aleksandrov, and S. M. Stishov, Phys. Rev. B **32**, 484 (1985).
[17]P. Loubeyre, R. LeToullec, M. Hanfland, L. Ulivi, F. Datchi, and D. Hausermann, Phys. Rev. B **57**, 10403 (1998).
[18]M. Ross, H. K. Mao, P. M. Bell, and J. A. Xu, J. Chem. Phys. **85**, 1028 (1986).
[19]L. W. Finger, R. M. Hazen, G. Zou, H. K. Mao, and P. M. Bell, Appl. Phys. Lett. **39**, 892 (1981).
[20]A. Dewaele, P. Loubeyre, and M. Mezouar, Phys. Rev. B **70**, 094112 (2004).
[21]P. E. Blöchl, Phys. Rev. B **50**, 17953 (1994).
[22]G. Kresse and J. Furthmüller, Comput. Mater. Sci. **6**, 15 (1996); Phys. Rev. B **54**, 11169 (1996); G. Kresse and D. Joubert, *ibid*. **59**, 1758 (1999).
[23]Y. Wang and J. P. Perdew, Phys. Rev. B **44**, 13298 (1991); J. P. Perdew, J. A. Chevary, S. H. Vosko, K. A. Jackson, M. R. Pederson, D. J. Singh, and C. Fiolhais, *ibid*. **46**, 6671 (1992).
[24]N. D. Mermin, Phys. Rev. A **137**, 1441 (1965).
[25]J. M. Haile, *Molecular Dynamics Simulation: Elementary Methods* (Wiley, New York, 1997).
[26]D. E. Gray, *American Institute of Physics Handbook*, 2nd ed. (McGraw-Hill, New York, 1963).
[27]J. P. Perdew and A. Zunger, Phys. Rev. B **23**, 5048 (1981).
[28]O. L. Anderson, *Equations of State of Solids in Geophysics and Ceramic Science* (Oxford University Press, Oxford, 1995).
[29]F. Birch, J. Geophys. Res. **91**, 4949 (1986).
[30]S. Ono, J. P. Brotholt, D. Alfè, M. Alfredsson, and G. D. Price, J. Appl. Phys. **103**, 023510 (2008).
[31]O. L. Anderson, D. G. Isaak, and S. Yamamoto, J. Appl. Phys. **65**, 1534 (1989).
[32]P. I. Dorogokupets, Phys. Chem. Miner. **37**, 667 (2010).
[33]A. Dewaele, P. Loubeyre, F. Occelli, M. Mezouar, P. I. Dorogokupets, and M. Torrent, Phys. Rev. Lett. **97**, 215504 (2006).
[34]A. B. Belonoshko, Condens. Matter. Phys. **13**, 23605 (2010).